Journal Name

ARTICLE TYPE

Cite this: DOI: 00.0000/xxxxxxxxxx

Effect of an axial ligand on the self-assembly of molecular platforms†

Chao Li,[a] Xiangzhi Meng,[a] Alexander Weismann,[a] Jan-Simon von Glasenapp,[b] Sebastian Hamer,[b] Feifei Xiang,[c] Carlo A. Pignedoli,[c] Rainer Herges,[b] and Richard Berndt[a*]

Received Date
Accepted Date

DOI: 00.0000/xxxxxxxxxx

Received Date
Accepted Date

DOI: 00.0000/xxxxxxxxxx

Sub-monolayer amounts of trioxatriangulenium (TOTA) molecules functionalized with biphenyl on Ag(111) were investigated with scanning tunneling microscopy. The molecule is comprised of a rod-shaped axial ligand and a triangular platform that tends to form hydrogen bonds in arrays. Two superstructures are observed, a hexagonal tiling and a phase of molecular double rows. While the former structure matches previous observations from other functionalized TOTA molecules the latter one was unexpected. Aided by density functional theory results we analyse the observed intramolecular contrast and present a model of the new phase. We discuss possible interaction mechanisms underlying the molecular pattern.

Molecular self-assembly on surfaces is interesting for the mass fabrication of artificial nanostructures.[1–3] Numerous patterns have been prepared at solid surfaces and liquid-solid interfaces by manipulating the interactions among molecules and with the substrate.[4–12] Among the molecule-molecule interactions, hydrogen bonding is often used because of its selectivity and directionality.[13–15] The resulting structures can easily be tuned by molecular coverage, sample temperature, and substrate materials.[16–18] Most of the reported hydrogen-bonded structures on surfaces involved planar molecules. The assembly of three-dimensional architectures, however, appears to be important for fabricating complex functional nanostructures at surfaces.

[a] *Institut für Experimentelle und Angewandte Physik, Christian-Albrechts-Universität zu Kiel, 24098 Kiel, Germany; E-mail: berndt@physik.uni-kiel.de*
[b] *Otto-Diels-Institut für Organische Chemie, Christian-Albrechts-Universität zu Kiel, 24098 Kiel, Germany.*
[c] *nanotech@surfaces Laboratory, EMPA, Swiss Federal Laboratories for Materials Science and Technology, 8600 Dübendorf, Switzerland.*

Below we focus on triangular trioxatriangulenium (TOTA) molecules, which are capable of hosting various axial ligands and usually are suitable for the deposition on metal surfaces.[19–23] While pristine TOTA platforms are charged and thus repell each other, hexagonal or honeycomb arrays are observed on Au(111) or Ag(111) when axial CH_3, H, or C_2H ligands are present.[24,25] Other patterns have been observed when bulky ligands were used, whose lateral dimensions exceeded those of the TOTA platform.[20] Plenty of other triangular, but essentially planar, molecules have been studied.[26–33] For example, trimesic acid (TMA) molecules form various porous networks with honeycomb or hexagonal symmetries.[34–37] As an exception from this rule, a structure of alternating stripes of TMA molecules was reported from a liquid-solid interface.[38] All molecules within a stripe exhibited the same orientation whereas the stripes were related by a 180° rotation.

Here, we report scanning tunneling microscopy (STM) data and density functional theory (DFT) studies of biphenyl-functionalized TOTA on Ag(111). In addition to hexagonal tiling we find a majority phase of double chains with lower molecular density. In the latter structure, intriguing intramolecular contrasts are observed. According to DFT calculations for isolated biphenyl-TOTA on Ag(111) the image contrast reflects the orientation of the top part of the biphenyl moiety, which stands almost vertically on the TOTA platform. Manipulation experiments are consistent with this interpretation. We analyse the geometric arrangement of the TOTA subunits and propose a model of hydrogen-bonded double chains.

A typical STM image of a sub-monolayer amount of biphenyl-TOTA on Ag(111) is presented in Figure 1b). The 50×50 nm^2 overview shows two phases of self-assembled molecules on the

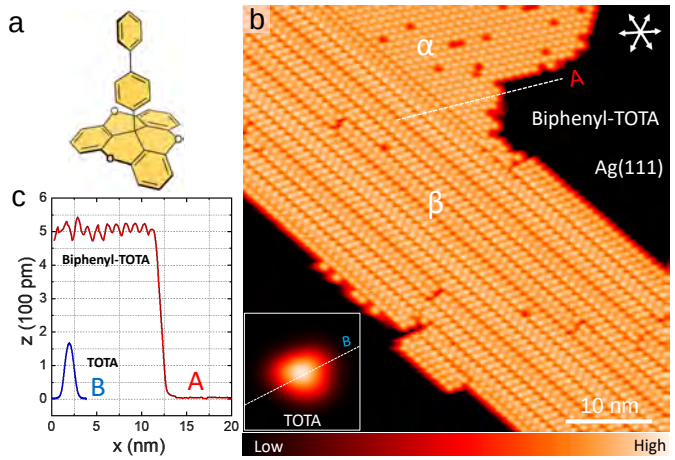

Fig. 1 a) Model of biphenyl-TOTA. b) STM constant current topograph of a biphenyl-TOTA monolayer on Ag(111). The sixfold arrow represents the surface direction $[1\bar{1}0]$ of Ag(111). The image reveals two molecular phases. c) Isolated fragment attributed to a TOTA molecule. d) Height profiles along the dotted lines in (b) and (c) for biphenyl-TOTA and TOTA. Imaging parameters: Sample voltage $V = 1$ V, current $I = 10$ and 40 pA in b and d, respectively.

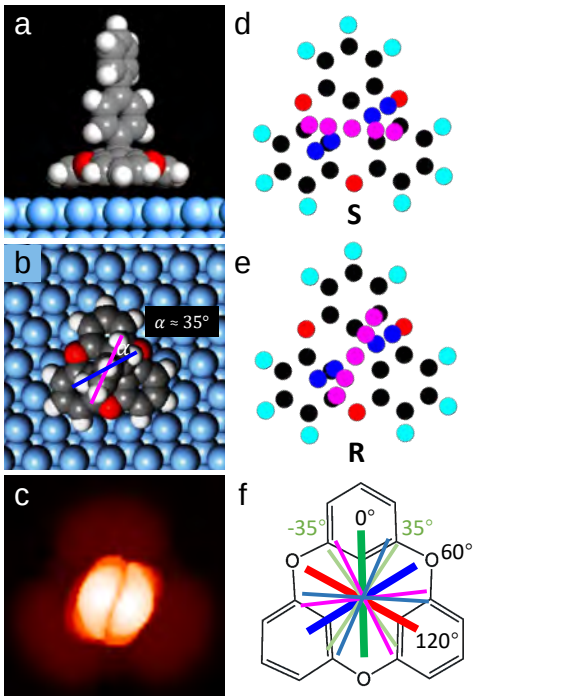

Fig. 2 a) Side view of the optimized geometry of biphenyl-TOTA molecule on Ag(111). b) Corresponding top view. The angle between the upper and lower phenyl subunits is $\approx 35°$. c) Simulated constant current STM image of single biphenyl-TOTA at –1 V. d) and e) Two chiral enantiomers of biphenyl-TOTA. The pink and blue dots represent the C atoms of the upper and lower phenyl rings, respectively. H atoms at the phenyls are not shown. C, O, and H atoms of the platforms are shown in black, red, and light blue. f) Thick lines (green, red, blue) indicate the three possible orientations of the lower phenyl ring, which H-binds to an O atom of the TOTA platform. Thin lines in matching colors show the possible 6 orientations of the upper phenyl, which is imaged by the STM.

surface. Less than 10% of all adsorbed molecules are found in a hexagonal structure, which we denote phase α. This structure is not surprising and similar patterns were previously observed from triangular functionalized TOTA molecules on C_3 symmetric fcc(111) surfaces.[19–25,39] The predominant phase β, however, is a superstructure of apparent dimer chains.

Height measurements were performed to detect a possible fragmentation of biphenyl-TOTA. Cross-sectional profiles along the lines indicated in Figures 1 b and the inset are shown in Figure 1c. The molecules in phases α and β exhibit similar apparent heights of ≈ 0.55 nm at $V = 1.0$ V while an isolated triangular fragment displays a height of ≈ 0.17 nm. The latter value is close to the measured 0.21 nm height of TOTA molecules on Au(111).[24] We therefore attribute the fragment to a TOTA molecule while the taller and much more abundant molecules in phases α and β are intact biphenyl-TOTA.

For a more detailed analysis of the STM data it is helpful to first consider the calculated structure and a STM image of an isolated biphenyl-TOTA molecule on Ag(111). Figures 2a and b show side and top views of an optimized molecular model. The TOTA platform is adsorbed planar on the substrate as previously observed and expected owing to the large van der Waals interaction with the metal.[24] The biphenyl moiety stands vertically on the TOTA unit. We find a torsion angle of $35° \pm 3°$ between the phenyl rings, which may be attributed to a compromise between the steric repulsion of hydrogen atoms and the planarization driven by conjugation. One H atom of the lower phenyl ring points toward one of the three oxygen atoms in the platform reflecting a C–H–O bond with a C–O distance of 335 pm. Previous gas phase calculations of biphenyl-TOTA led to closely related results.[39]

Because of the large height of the biphenyl ligand STM images are not directly sensitive to the TOTA platform and its orientation on the surface. They rather reveal the orientation of the upper phenyl moiety as shown in Figure 2c. This constant current image simulated for a sample voltage $V = -1$ V exhibits two equivalent protrusions,[40,41] which are due to the π-electron system. The nodal line separating them thus is parallel to the upper phenyl ring. A similar result was obtained for $V = 1$ V.

In addition to the calculated structure presented so far, a number of geometries are expected that are related by symmetry. First, the arrangement of the biphenyl on the platform is chiral. Consequently, two enantiomers are expected as shown in Figures 2d and e. The upper phenyl subunit (pink dots) may be rotated clockwise or anticlockwise with respect to the lower one (blue dots). Second, the lower phenyl, which H-bonds to an O of the platform, may exhibit three different orientations (Figure 2f). Third, the platform may be adsorbed as shown or rotated by 180° around the surface normal.

An enlarged view of the hexagonal phase α is shown in Figure 3a. Hexagonal order with a nearest neighbor distance of 1.04 nm is observed although a defect (dark spot) is present. The primitive cell of this structure is rotated by 13.9° with respect to the substrate lattice observed in atomic resolution images of molecul-free areas. In other words, the molecules form the same $\sqrt{13} \times \sqrt{13}$ R13.9° mesh previously observed from methyl-

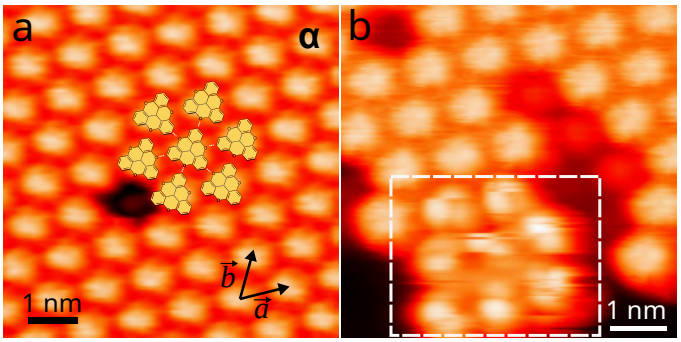

Fig. 3 a) Enlarged topograph of phase α. $\vec{a}$ and $\vec{b}$ are primitive vectors of the superstructure. Models of seven TOTA platforms – biphenyl not shown – are overlaid on the topograph. b) STM image of an island edge of the hexagonal phase. A dashed box indicates molecules that display imaging artifacts and possibly some internal structure. a) 1 V, 100 pA; b) 0.5 V, 60 pA.

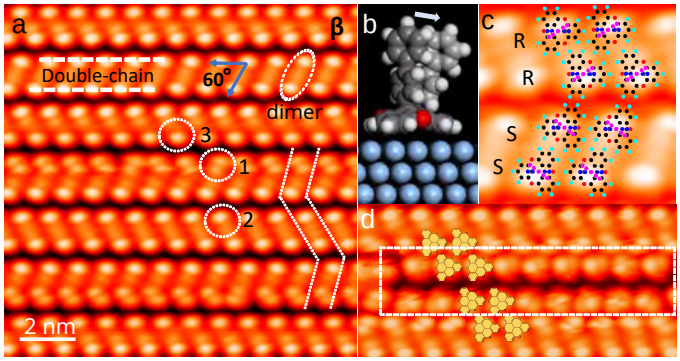

Fig. 4 a) STM topograph of the double-chain phase β. Circles mark three different configurations 1, 2, and 3 of biphenyl-TOTA molecules. b) Illustration of a tilted biphenyl subunit. c) Proposed model of phase β overlaid on the top two double chains of the image in a. Pink and blue circles represent the upper phenyl ring and the lower phenyl ring, respectively. The platform orientation changes by 180° between the two double chains. In addition, S and R enantiomers are involved. It should be noted that the data would also be consistent with all platform orientations rotated by 180° while keeping the chiralities fixed. d) Defect area in phase β with a model of the molecular pattern. Imaging parameters: 1 V, 10 pA.

TOTA[25]. A model of the pattern of the platforms (ligands not shown) is overlaid in Figure 3a. The triangular platforms are arranged in a corner-to-side geometry. There is one O atom per side and each of them is involved in hydrogen bonding to a corner of a neighbor molecule. Each TOTA is thus involved in six H bonds.

The structure of phase α requires that all triangles be oriented in the same direction. Because of the 180° symmetry mentioned aboved, this may lead to two domains, each with identically oriented platforms. The image contrast being dominated by the biphenyl, however, the orientation of the triangles is not resolved in the experimental topographs. For this reason, the model shown in Fig. 3a may also be rotated by 180°.

The internal structure expected from the calculations and observed in the double chains (*vide infra*) is not resolved in the hexagonal arrays. Apparently the ligand orientation is unstable under the influence of the STM tip. At island edges or slightly disordered areas (dashed circle in Figure 3b), the effect of the tip occasionally is apparent in the form of stripes along the fast scan direction of the tip. Some indication of the expected two-lobed pattern is also observed in these areas. Purely thermally induced rotation seems unlikely because the barrier for rotation should not easily be overcome at the temperature of the experiment. Gas-phase calculations of the molecule (substrate neglected) indicate barrier heights for the rotations of the the upper and lower phenyl rings of > 60 and 11 meV, respectively.[39] Although the interaction with a Ag substrate may modify in particular the latter barrier height thermal rotation is unlikely at the cryogenic temperature of the measurements ($k_BT \approx 0.4$ meV). As to rotation induced with the STM tip, the different barrier heights suggest that rotation of the entire biphenyl is more likely than rotation of the upper phenyl ring alone. The barrier heights also suggest that the phenyl subunits may rotate during the preparation and annealing of the molecular layer.

A STM image of phase β is presented in Figure 4a. From inspection of island edges along with the feature sizes in the topographs it becomes clear which image features correspond to a molecule. Intriguingly, we find three forms of appearance of biphenyl-TOTA, which are indicated by dotted circles in the figure. Form 1 displays two almost identical protrusions separated by a nodal line as expected from the calculations. In forms 2 and 3, however, height differences between the protrusions are obvious. Pairs of molecules may be viewed as dimers which in turn form double chains. The double chains seem to be separated by grooves. From an analysis of sufficiently large areas, using equivalent protrusions, we find that the molecular density in phase β (0.98 nm^{-2}) is lower than in phase α (1.11 nm^{-2}). This reduction is caused by a uniaxial expansion ($\approx 13\%$) in the direction perpendicular to the chains. Moreover, we observe angles of $\approx 60°$ in the chains as indicated in Figure 4a. It should be noted, however, that this angle may slightly deviate from the angle in the platform arrangement because the imaged top phenyls may exhibit different lateral offsets from the centers of the platforms.

For further analysis we first consider the differences in apparent height between the two protrusions of each form. It is important to keep in mind that the color scheme used for the STM images tends to visually overemphasize such differences. The measured values are 12, 53, and 73 pm for forms 1 to 3, which should be compared to the vertical extension of biphenyl (≈ 820 pm) and the lateral separation of the protrusions (≈ 380 pm). If these differences are entirely caused by a tilting of the biphenyl moiety, the corresponding deviations of the ligand from a perpendicular orientation are 1.6, 3.7, and 8.7°, respectively.

Taking the tilt angles into account, we estimate the distances between the centers of the platforms within double chains to be similar or possibly slightly smaller than the intermolecular distance in phase α (1.04 nm). This leads us to propose the following model of phase β (Figure 4c). Within each double chain the molecular pattern is identical to the arrangement in phase α, although a minor contraction along the direction perpendicular to the chains may be present. From double chain to double chain the orientations of the platforms alternate.

This model is consistent with the observed uniaxial expansion of phase β and the intermolecular distances within each double chain. H-bonding does not occur between double chains because of the alternating orientations of the platforms, the interaction between double chains is correspondingly reduced, and their distance is expected to increase as observed in the data.

As a further test of the proposed models, it is helpful to consider an area of phase β that contains a line defect (Figure 4d, white rectangle), namely an apparent groove in the double chain arrangement. In the defect area, two molecular chains are offset toward the neighboring chains above and below the groove. This local configuration matches the molecular pattern of phase α. Similar to the observations made in phase α, the ligand orientation in the two displaced chains is unclear, presumably because of an interaction with the STM tip. This change in image stability confirms that the interaction in double chains helps to orient the ligands in a regular pattern.

We note that phase α comprises a single orientation of the platforms. Its formation thus requires molecular diffusion over large distances or a sufficiently low barrier for the rotation of the platforms on the substrate. Phase β relaxes the requirements because the orientations of the platforms alternate. In addition, the structure is a racemic mixture.

Based on the intramolecular contrast the orientations of the upper phenyl subunits may be evaluated. The data suggest that the molecules within each double chain correspond to a single enantiomer and are oriented parallel to each other. The lower phenyls consequently point along the chain direction. In the model in Figure 4c S and R enantiomers are combined with triangular platforms that point to the left and the right. However, a model with the platforms rotated by 180° is also consistent with the data.

All lower phenyl rings (blue) in the model are oriented along the chain direction to achieve best match between the nodal lines in the image and the upper phenyl (red). This orientation enables a H bond between the lower phenyl and one of the two oxygen atoms of the platform that are involved in H bonds to neighbors. Our calculations for biphenyl TOTA dimers on a layer of Ag indeed showed that these O atoms are slightly favored for binding the ortho-H of the lower phenyl subunit.

The connection between the orientation of the upper phenyl rings and the STM image contrast can be used to visualize induced rotations. Figure 5a shows a time series of the current recorded above a molecule in form 1 at $V = 1.7$ V. Clear two-level fluctuations are observed. Imaging before and after such fluctuations (Figures 5b and c) reveals that the biphenyl reversibly changes its orientation by 60°. The two orientations observed are consistent with bonds of the ortho H of the lower phenyl to two equivalent O atoms of the TOTA platform, namely those ones that are involved in H-bonding to neighbor platforms. As mentioned above, these O atoms are slightly prefered compared to the lone O that is located close to the groove separating double chains.

To discuss the driving force for the formation of phase β, it is useful to first recall some results obtained for methyl-TOTA. That compound was observed to aggregate into a hexagonal pattern similar to phase α.[24] The data suggested that the platform-platform interaction is decisive in that case with each TOTA subunit being involved in six identical hydrogen bonds. By replacing methyl with biphenyl, a different pattern is induced. We find a uniaxial expansion and an apparent dimerization. In view of the small lateral extension of biphenyl, which is expected to prevent steric interactions between neighboring ligands, this drastic effect is astonishing. We therefore considered less direct forms of interaction. To evaluate their significance, we first estimated the energy required to tilt a biphenyl subunit on the TOTA platform. According to our gas-phase calculations for a biphenyl-TOTA dimer, the energy required to bend a biphenyl group is less than 10 meV for bending angles smaller than 3°, and reaches ≈ 20 meV at 8° (Supplementary information, Figure S8). When the substrate is included in the calculations we find ≈ 57 meV for a bending angle of ≈ 8.7° (Supplementary information, Figures S4 – S7).

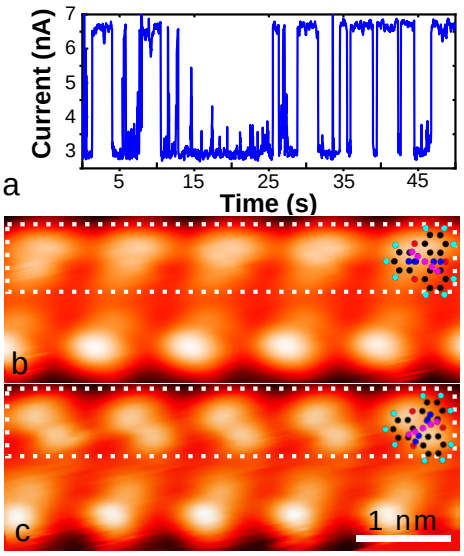

Fig. 5 a) Time series of the current recorded above biphenyl at $V = 1.7$ V. There are two-level fluctuations between 2.7 and 6.6 nA. b and c) Switching of the orientations of biphenyl subunits of five targeted molecules marked by a rectangle. The molecular orientations inferred are indicated by overlaid models. Imaging parameters: 1 V, 10 pA.

First, the biphenyl ligands may exert van der Waals forces on their neighbors. Since no published results for biphenyl appear to be available, we calculated the interaction energy between two phenyl rings and found no significant energy at a distance of 1 nm (Supplementary information, Figures S1–S3). We therefore tentatively disgard the possibility that dispersion interaction is the cause of the apparent dimerization.

Second, the intramolecular H-bond of the lower phenyl may singles out one particular O atom of the platform. Our calculations for phenyl-TOTA dimers indeed suggest that a H atom of the lower phenyl ring prefers a position close to the particular O atom of TOTA that is involved in a H-bond to the neighbor platform. For TOTA–TOTA distances of 0.94 and 1.04 nm we calculate energy differences of ≈ 0.45 kcal/mol (20 meV) and less than 0.125 kcal/mol (5 meV), respectively (Supplementary information, Figure S8). These energies are of the same order of magnitude as the estimated elastic energies and therefore may be considered as the interaction leading to dimerization.

In conclusion, axial biphenyl groups profoundly affect the self-assembly of triangular trioxatriangulenium (TOTA) molecules on Ag(111). While hexagonal tiling was observed from TOTA derivatives and understood in terms of direct interactions between the TOTA platforms via H bonds, biphenyl TOTA molecules predominantly arrange into a complex pattern of double chains. A model describing important aspects of this pattern is presented. The data suggest that weak dispersion forces that indirect interactions mediated by H bonds may be underlying the unexpected self-assembly pattern. The results highlight some of the challenges in understanding the self-assembly of three-dimensional molecules at surfaces.

Acknowledgments

C. P. acknowledges funding by the NCCR MARVEL of the Swiss National Science Foundation (grant no. 51NF40-205602) and computational resources from the Swiss National Supercomputing Centre (CSCS) under project ID s1141. F. X. acknowledges support via a Walter Benjamin Fellowship from Deutsche Forschungsgemeinschaft. C. L. thanks the Humboldt Foundation for a postdoc fellowship.

Conflicts of interest

There are no conflicts to declare.

Notes and references

1 R. Otero, J. M. Gallego, A. L. V. de Parga, N. Martin and R. Miranda, *Adv. Mater.*, 2011, **23**, 5148–5176.
2 R. Gutzler, L. Cardenas and F. Rosei, *Chem. Sci.*, 2011, **2**, 2290–2300.
3 D. P. Goronzy, M. Ebrahimi, F. Rosei, Arramel, Y. Fang, S. De Feyter, S. L. Tait, C. Wang, P. H. Beton, A. T. Wee *et al.*, *ACS Nano*, 2018, **12**, 7445–7481.
4 E. Gomar-Nadal, J. Puigmartí-Luis and D. B. Amabilino, *Chem. Soc. Rev.*, 2008, **37**, 490–504.
5 H. Liang, Y. He, Y. Ye, X. Xu, F. Cheng, W. Sun, X. Shao, Y. Wang, J. Li and K. Wu, *Coord. Chem. Rev.*, 2009, **253**, 2959–2979.
6 Q. Fan, C. Wang, L. Liu, Y. Han, J. Zhao, J. Zhu, J. Kuttner, G. Hilt and J. M. Gottfried, *J. Phys. Chem. C*, 2014, **118**, 13018–13025.
7 M. Stöhr, S. Boz, M. Schär, M.-T. Nguyen, C. A. Pignedoli, D. Passerone, W. B. Schweizer, C. Thilgen, T. A. Jung and F. Diederich, *Angew. Chem. - Int. Ed.*, 2011, **50**, 9982–9986.
8 Y. Xu, T. Chen and D. Wang, *J. Phys. Chem. C*, 2021, **125**, 15354–15362.
9 S. Scherb, A. Hinaut, R. Pawlak, J. Vilhena, Y. Liu, S. Freund, Z. Liu, X. Feng, K. Müllen, T. Glatzel *et al.*, *Commun. Mater.*, 2020, **1**, 1–7.
10 R. Sarkar, K. Guo, C. N. Moorefield, M. J. Saunders, C. Wesdemiotis and G. R. Newkome, *Angew. Chem. - Int. Ed.*, 2014, **53**, 12182–12185.
11 C. Li, X. Zhang, N. Li, Y. Wang, J. Yang, G. Gu, Y. Zhang, S. Hou, L. Peng, K. Wu *et al.*, *J. Am. Chem. Soc.*, 2017, **139**, 13749–13753.
12 H. Kong, Y. Qian, X. Liu, X. Wan, S. Amirjalayer and H. Fuchs, *Angew. Chem. - Int. Ed.*, 2020, **59**, 182–186.
13 X.-J. Luan, Y.-Y. Wang, D.-S. Li, P. Liu, H.-M. Hu, Q.-Z. Shi and S.-M. Peng, *Angew. Chem. - Int. Ed.*, 2005, **44**, 3864–3867.
14 C. Li, R. Li, Z. Xu, J. Li, X. Zhang, N. Li, Y. Zhang, Z. Shen, H. Tang and Y. Wang, *J. Am. Chem. Soc.*, 2021, **143**, 14417–14421.
15 S. Karan, Y. Wang, R. Robles, N. Lorente and R. Berndt, *J. Am. Chem. Soc.*, 2013, **135**, 14004–14007.
16 F. Schreiber, *Prog. Surf. Sci.*, 2000, **65**, 151–257.
17 T. Kudernac, S. Lei, J. A. Elemans and S. De Feyter, *Chem. Soc. Rev.*, 2009, **38**, 402–421.
18 D. Li, L. Sun, Y. Ding, M. Liu, L. Xie, Y. Liu, L. Shang, Y. Wu, H.-J. Jiang, L. Chi *et al.*, *ACS Nano*, 2021, **15**, 16896–16903.
19 S. Kuhn, U. Jung, S. Ulrich, R. Herges and O. Magnussen, *Chem. Commun.*, 2011, **47**, 8880–8882.
20 F. L. Otte, S. Lemke, C. Schütt, N. R. Krekiehn, U. Jung, O. M. Magnussen and R. Herges, *J. Am. Chem. Soc.*, 2014, **136**, 11248–11251.
21 T. Jasper-Tönnies, A. Garcia-Lekue, T. Frederiksen, S. Ulrich, R. Herges and R. Berndt, *Phys. Rev. Lett.*, 2017, **119**, 066801.
22 T. Jasper-Tönnies, A. Garcia-Lekue, T. Frederiksen, S. Ulrich, R. Herges and R. Berndt, *J. Phys. Condens. Matter*, 2019, **31**, 18LT01.
23 T. Jasper-Toennies, M. Gruber, S. Johannsen, T. Frederiksen, A. Garcia-Lekue, T. Jäkel, F. Roehricht, R. Herges and R. Berndt, *ACS Nano*, 2020, **14**, 3907–3916.
24 T. Jasper-Tönnies, I. Poltavsky, S. Ulrich, T. Moje, A. Tkatchenko, R. Herges and R. Berndt, *J. Chem. Phys.*, 2018, **149**, 244705.
25 T. Jasper-Tönnies, M. Gruber, S. Ulrich, R. Herges and R. Berndt, *Angew. Chem.*, 2020, **132**, 7074–7083.
26 Y. Shen, K. Deng, S. Yang, B. Qin, S. Cheng, N. Zhu, J. Ding, D. Zhao, J. Liu, Q. Zeng *et al.*, *Nanoscale*, 2014, **6**, 7221–7225.
27 M. Bao, X. Wei, L. Cai, Q. Sun, Z. Liu and W. Xu, *Phys. Chem. Chem. Phys. PCCP*, 2017, **19**, 18704–18708.
28 P. Szabelski, W. Rżysko and D. Nieckarz, *Top. Catal.*, 2018, **61**, 1218–1226.
29 Q.-Y. Chen, J.-J. Song, L. Jing, K. Huang, P. He and H. Zhang, *Chin. Phys. B*, 2020, **29**, 026801.
30 Z. Yang, L. Fromm, T. Sander, J. Gebhardt, T. A. Schaub, A. Görling, M. Kivala and S. Maier, *Angew. Chem. - Int. Ed.*, 2020, **59**, 9549–9555.
31 Y. Fang, B. D. Lindner, I. Destoop, T. Tsuji, Z. Zhang, R. Z. Khaliullin, D. F. Perepichka, K. Tahara, S. D. Feyter and Y. Tobe, *J. Am. Chem. Soc.*, 2020, **142**, 8662–8671.
32 G. Feng, Y. Shen, Y. Yu, Q. Liang, J. Dong, S. Lei and W. Hu, *Chem. Commun.*, 2021, **57**, 2065–2068.
33 H. Shan, L. Zhou, W. Ji and A. Zhao, *J. Phys. Chem. Lett.*, 2021, **12**, 10808–10814.
34 A. Dmitriev, N. Lin, J. Weckesser, J. Barth and K. Kern, *J. Phys. Chem. B*, 2002, **106**, 6907–6912.
35 M. Lackinger, S. Griessl, W. M. Heckl, M. Hietschold and G. W. Flynn, *Langmuir*, 2005, **21**, 4984–4988.
36 K. G. Nath, O. Ivasenko, J. A. Miwa, H. Dang, J. D. Wuest, A. Nanci, D. F. Perepichka and F. Rosei, *J. Am. Chem. Soc.*, 2006, **128**, 4212–4213.
37 Y. Ye, W. Sun, Y. Wang, X. Shao, X. Xu, F. Cheng, J. Li and K. Wu, *J. Phys. Chem. C*, 2007, **111**, 10138–10141.
38 N. T. Ha, T. G. Gopakumar, R. Gutzler, M. Lackinger, H. Tang and M. Hietschold, *J. Phys. Chem. C*, 2010, **114**, 3531–3536.
39 S. Hamer, J.-S. von Glasenapp, F. Röhricht, C. Li, R. Berndt and R. Herges, *Chem.–Eur. J.*, 2021, **27**, 17452–17458.
40 G. Pizzi, A. Cepellotti, R. Sabatini, N. Marzari and B. Kozinsky, *Comput. Mater. Sci.*, 2016, **111**, 218–230.
41 A. V. Yakutovich, K. Eimre, O. Schütt, L. Talirz, C. S. Adorf, C. W. Andersen, E. Ditler, D. Du, D. Passerone, B. Smit, N. Marzari, G. Pizzi and C. A. Pignedoli, *Comput. Mater. Sci.*, 2021, **188**, 110165.